

# Field induced topological phase transition from three-dimensional Weyl semimetal to two-dimensional massive Dirac metal in $\text{ZrTe}_5$

Guolin Zheng<sup>1\*</sup>, Xiangde Zhu<sup>1\*</sup>, Jianwei Lu<sup>1</sup>, Wei Ning<sup>1</sup> §, Hongwei Zhang<sup>1</sup>,  
Wenshuai Gao<sup>1</sup>, Yuyan Han<sup>1</sup>, Jiyong Yang<sup>1</sup>, Haifeng Du<sup>1</sup>, Kun Yang<sup>3</sup> §, Yuheng  
Zhang<sup>1</sup> and Mingliang Tian<sup>1,2</sup> §

<sup>1</sup>*High Magnetic Field Laboratory, Chinese Academy of Sciences, Hefei 230031, Anhui, the People's Republic of China; Department of physics, University of Science and Technology of China. Hefei 230026, the People's Republic of China*

<sup>2</sup>*Collaborative Innovation Center of Advanced Microstructures, Nanjing University, Nanjing 210093, the People's Republic of China*

<sup>3</sup>*National High Magnetic Field Laboratory, Florida State University, Tallahassee, Florida 32306-4005, USA*

\* Those authors contribute equally to this work.

§To whom correspondence should be addressed. E-mail: kunyang@magnet.fsu.edu (K.Y.), ningwei@hmfl.ac.cn (W.N.), tianml@hmfl.ac.cn (M.T).

## Abstract

Symmetry protected Dirac semimetal can be transformed into a Weyl semimetal by breaking the protecting symmetry, leading to many exotic quantum phenomena such as chiral anomaly<sup>1-9</sup>, anomalous Hall effect<sup>10-13</sup>. Here we show that, due to the large Zeeman  $g$  factor and small band width along  $b$ -axis in Dirac semimetal  $\text{ZrTe}_5$ , a magnetic field of about 8 T along  $b$ -axis direction can annihilate the Weyl points and open up a two-dimensional (2D) Dirac mass gap, when the Zeeman splitting exceeds the band width along  $b$ -axis. This is manifested by a sharp negative MR (nMR) above 8T, which is due to additional carriers induced by the orbital splitting of the zeroth Landau level associated with the 2D Dirac point, which is decedent of the original Weyl points. Further evidence of the additional carriers is provided by the Hall effect and different anisotropic magnetoresistance (AMR) in low and high field regions. Our experiment reveals a topological quantum phase transition of field induced Weyl points annihilation in Dirac semimetal  $\text{ZrTe}_5$ .

Three-dimensional (3D) Dirac and Weyl semimetals have attracted extensive attentions recently, due to their exotic transport properties and potential impacts on information technology. Dirac semimetal, holding a pair of Weyl points coinciding at the Dirac point, is usually unstable unless protected by some special symmetries such as time reversal symmetry (TRS), spatial inversion symmetry as well as crystalline point-group symmetry<sup>14-17</sup>. Thus a magnetic field  $B$ , which breaks time reversal symmetry, can turn a Dirac semimetal to a Weyl semimetal, which is more robust since the Weyl points can only disappear by annihilation of pairs with opposite topological charges<sup>18</sup>. The recently discovered Dirac semimetal phase in layered material  $ZrTe_5$  provides an ideal platform to explore the exotic quantum phenomena in TRS-broken Dirac semimetals, since in this layered material a modest magnetic field can drive the system into the quantum limit<sup>19, 20</sup>. In addition, compared with other topological semimetals, layered material  $ZrTe_5$  has very weak interlayer coupling<sup>21</sup> as well as large Zeeman  $g$  factor according to recent magneto infrared spectroscopy study<sup>19</sup>. A small band width in the interlayer direction can be anticipated due to the weak interlayer coupling, which allows for interplay with the Zeeman splitting when a sufficiently strong magnetic field is applied in the interlayer direction. Some unusual quantum phenomena can be anticipated due to the large Zeeman splitting, especially when it exceeds the band width in the interlayer direction, a regime never explored experimentally before.

In this paper, we show that due to the weak interlayer coupling in  $ZrTe_5$ , a critical magnetic field  $B^*$  of about 8 T applied in the interlayer direction ( $b$ -axis direction)

will generate a large enough Zeeman splitting comparable to the band width in this direction. Above 8 T, the large Zeeman splitting will exceed the band width and quench dispersion in this direction, and turn the 3D (massless) Weyl points into a *massive* 2D Dirac point by annihilating the Weyl points when they reach Brillouin zone boundary. Such a topological quantum phase transition is revealed by a sharp negative magnetoresistance (nMR) when  $B$  exceeds 8 T. We argue this is due to the orbital splitting of the massive 2D Dirac point, when the system is approaching to the zeroth Landau Level (LL). Such splitting induces additional carriers, which is manifested by the significant change in Hall effect at the same field, and strong sensitivity of the observed effects to the direction of the magnetic field. Further evidence of such orbital splitting is demonstrated by the different anisotropic magnetoresistance (AMR) in low and high field regions. Such magnetic field induced annihilation of Weyl points has never been observed before, and is expected to stimulate further research in topological quantum phase transition in topological semimetal under high magnetic field.

Layered materials  $\text{ZrTe}_5$  has been demonstrated to be a 3D Dirac semimetal recently by magneto-infrared spectroscopy study<sup>19,22</sup>, ARPES<sup>2</sup> and electrical transport experiments<sup>2, 20</sup>. In  $\text{ZrTe}_5$ , Zr atoms lie at the centers of right trigonal prisms of Te atoms stacked along the  $a$ -axis, while the parallel chains of trigonal prisms are coupled in the  $c$ -axis direction via zigzag chains of Te atoms to form two-dimensional  $a$ - $c$  plane, then stacked along the  $b$ -axis into a crystal<sup>23</sup>. We performed transport measurements in different single crystal  $\text{ZrTe}_5$  samples (S1-S4), and the current is

applied along  $a$ -axis, which is the most conductive direction.

Fig. 1(a) shows the magnetoresistance (MR) at various temperatures with magnetic field applied along  $b$ -axis. Below 20 K, the MR exhibits strong Shubnikov–de Hass (SdH) oscillations and the oscillations can be tracked down to as low as 1 T at 2 K, demonstrating high mobility of our sample. More interestingly, at 2 K the MR reaches a maximum at the critical field  $B^*$  of about 8 T, followed by a sharp drop. At the first glance of the MR curve, it seems that the sharp drop of the MR near 8 T belongs to the quantum oscillations or the Landau level (LL) splitting. However, with increasing temperature, the peak position of MR is found to shift toward the high field direction and disappears at  $T > 80$  K in our measured range. Such negative magnetoresistance (nMR) at high magnetic field region cannot be attributed to LL splitting or the quantum oscillation, because temperature can only smear the splitting and weaken the amplitudes of the SdH oscillations without shifting the peak position. Fig. 1(b) shows  $dR/dB$  under different temperatures. It shows that a moderate magnetic field of about 5 T can drive the system into the first LL  $n=1$ , and both the peak position of LL  $n=1$  and  $n=2$  are split into several sub-peaks at 2 K. Such split behavior of the LL can be attributed to the removal of the spin degeneracy due to the spin Zeeman splitting<sup>6, 19</sup>. As we will discuss in detail later, Zeeman splitting moves the Weyl points in momentum space, and transforms the system from a Dirac semimetal to a Weyl semimetal. As  $T$  increases, the splitting is gradually weakened by the thermal fluctuation and finally smeared out when  $T=20$  K. We also note that, in Fig. 1(b), the sharp dip on the left side of the dashed line (nMR region) moves to high field region

when T increases, which is sharply distinguished from the oscillation components in the low field region (on the right side of the dashed line), where the temperature only weakens the amplitude of the oscillations without shifting the peak position.

To have a better understanding of the SdH oscillation, we have tracked the angle dependent magnetoresistance (ADMR) at 2 K under different tilted angle with B rotating in both  $b$ - $a$  and  $b$ - $c$  planes, as shown in Figure 2(a) and 2(c) respectively. The tilted angle  $\theta$  or  $\varphi$  is defined between B and  $b$ -axis rotating in the  $b$ - $a$  or  $b$ - $c$  planes, respectively. The derivative,  $dR/dB$ , as a function of  $1/B_{\perp}$ , with  $B_{\perp} = B\cos(\theta$  or  $\varphi)$ , are presented in Fig.2(b) and 2(d). As we can see, the peak position of the MR in Fig. 2(a) and 2(c) moves to high field region as the tilted angle  $\theta$  or  $\varphi$  increased, and the MR becomes totally positive near  $\theta = 75^{\circ}$  or  $\varphi = 67^{\circ}$  in the studied range. Two features are noticed in Fig.2(b) and 2(d): (1) in the low field region the peaks of the SdH oscillations shift continuously with angles, as marked by the dark dashed arrows, indicating a nature of 3D Fermi surface. (2) As B increases, the LLs split into several sub-peaks and these sub-peaks exhibit an independent tendency with  $1/B_{\perp}$ , as marked by the red dashed arrows, revealing a highly anisotropic Zeeman splitting (anisotropic Zeeman g factor) mainly happens along  $b$ -axis direction, and a 2D nature of electron motion at high field.

The Zeeman splitting is  $\varepsilon = g\mu_B B$ , where  $g$  is the effective Landé g factor,  $\mu_B$  is the Bohr magneton. Usually, the  $g$  factor can be determined exactly by looking for the Landau level coincidence condition  $2g\mu_B B = \hbar\omega_c$  in a tilted magnetic field for two-dimensional electron gas<sup>24</sup>, where  $\omega_c$  is the cyclotron frequency. In our ZrTe<sub>5</sub>

single crystal, the 3D Fermi surface has an anisotropic  $g$  factor, making it hard to determine the  $g$  factor by this method. We know that the SdH oscillations are only resolved when the Landau level spacing ( $\hbar\omega_c$ ) is larger than the broadening of the Landau levels  $\mathcal{T} = \hbar/\tau_s$ , where  $\tau_s$  is the quantum lifetime<sup>25</sup>. That is  $\hbar eB_{onset}/m^* \geq \mathcal{T}$ , where  $m^*$  is the effective cyclotron mass and  $B_{onset}$  is the oscillation onset field. Similarly, the prerequisite for the observation of the Landau level splitting is  $\varepsilon = g\mu_B B_s \geq \mathcal{T}$ , and  $B_s$  is the critical field where the Landau level splitting is resolvable,  $\mu_B = e\hbar/2m_0$  with  $m_0$  the mass of electron. Thus we have the relationship  $g \approx 2(B_{onset} m_0 / B_s m^*)$ . The effective cyclotron mass has  $m^* \sim 0.026 m_0$  for  $a$ - $c$  plane carriers in ZrTe<sub>5</sub>, according to our recent study<sup>20</sup>. By this method, we have estimated the effective  $g$  factor of about 36, which is comparable with recent experiment<sup>19,26</sup>. While for  $B$  applied along  $a$ -axis or  $c$ -axis, the obtained effective cyclotron mass is much larger than that for  $B$  applied along  $b$ -axis. Since the Landau level splitting is not resolvable within 16 T for these two directions, making it hard to determine the effective  $g$  factor. However, we can provide an upper bound of the effective  $g$  factor with  $g \leq 4$  in these two directions. Such a large effective Zeeman  $g$  factor in interlayer direction hints large Zeeman splitting under high magnetic field, which might compete with band width in this direction due to the weak interlayer coupling in ZrTe<sub>5</sub>.

To reveal the potential interplay between Zeeman splitting and band width along  $b$ -axis direction, we have analyzed the Fermi energy and the band width in this direction. By analyzing the SdH oscillation in low field region, a single periodic

oscillation frequency  $F=4.85$  T with  $B$  applied along  $b$ -axis direction is obtained by Fast Fourier Transform (FFT), and correspondingly the Fermi surface radius for the  $a$ - $c$  plane carriers is about  $k_{ac} = 0.0125 \text{ \AA}^{-1}$ . For free electron model, the Fermi energy can be estimated by the relationship  $E_F = (\hbar k_{ac})^2 / 2M_{ac}$ , where  $M_{ac}$  is the effective cyclotron mass for  $a$ - $c$  plane carriers. Considering the ellipsoidal Fermi surface, the effective band mass  $m_b$  in principal axis ( $b$ -axis direction) can be calculated by the ellipsoidal model  $m_b = M_{bc} \cdot F_c / F_b$ , where  $M_{bc}$  is the effective cyclotron mass for  $b$ - $c$  plane carriers obtained by the SdH oscillation and  $F_c, F_b$  are the SdH frequencies for  $c$ -axis and  $b$ -axis respectively<sup>27</sup>. The Fermi wave vector in  $b$ -axis direction has  $k_b = m_b v_b / \hbar$  with  $v_b$  the Fermi velocity along  $b$ -axis direction. The obtained Fermi wave vector  $k_b$  is about  $0.14 \text{ \AA}^{-1}$  and the estimated Fermi energy  $E_F$  ranging from  $7 \text{ meV}$  to  $13 \text{ meV}$  for most of our samples. Considering the lattice constants in all three directions<sup>23</sup>,  $a = 3.98 \text{ \AA}$ ,  $b = 14.5 \text{ \AA}$  and  $c = 13.7 \text{ \AA}$ , thus the size of Brillouin zone along  $b$ -axis is about  $k = 0.21 \text{ \AA}^{-1}$  (from center to the boundary of the Brillouin zone). Supposing a linear dispersion relationship of the band structure, we can estimate the band width along  $b$ -axis,  $E_b = E_F \cdot \frac{k}{k_b}$ , which ranges from  $10 \text{ meV}$  to  $19 \text{ meV}$  for different samples of our bulk compounds. Around  $8$  T, the estimated Zeeman splitting energy  $g\mu_B B / 2$  is about  $9 \text{ meV}$ , which is comparable with the band width along  $b$ -axis direction. While above  $8$  T, the Zeeman splitting will exceed the band width along  $b$ -axis and quench the dispersion along this direction, driving the 3D Fermi surface to a quasi-2D Fermi surface in the high field region.

To gain further insight into the quasi-2D character in high field region, we consider the low-energy effective Hamiltonian of a single Weyl point. In the absence of the magnetic field:

$$H = \sum_{j=1}^3 v_j \sigma_j p_j. \quad (1)$$

Where  $p$  is momentum,  $\sigma$  are Pauli matrices corresponding to electron spin, and  $v_{j=1,2,3}$  are the components of Fermi velocity along the three axes. The Weyl point is chosen to be at  $k=0$ . While applying a magnetic field  $B$  along  $\hat{z}$ , due to the Zeeman effect, the 3<sup>rd</sup> term in Eq. (1) becomes:

$$H_z = (v_3 p_3 - \Delta_z) \sigma_3, \quad (2)$$

where  $\Delta_z = g\mu_B B/2$  is the Zeeman splitting. For small  $B$  and  $\Delta_z$ , it will shift the Weyl point to  $k = (0, 0, \Delta_z/v_3)$ . However, when  $B$  reaches certain critical value, the Weyl point reaches the Brillouin zone boundary and cannot move further. Beyond this point the coefficient of  $\sigma_3$  in Eq. (2) will never reach zero, and the electron energy will never be zero, thus the 3D Weyl point is lost. The  $\sigma_3$  term in Eq. (2), whose the coefficient is always non-zero, plays a role very similar to a Dirac mass for a 2D Dirac Hamiltonian.

Another way to understand this is the pair of Weyl points, initially split by the Zeeman field moving apart from each other (say from the Brillouin zone center), start to move toward each other as the Zeeman splitting becomes sufficiently strong due to the periodicity of the Brillouin zone, and eventually meet and annihilate each other at the zone boundary, as illustrated in Fig. 3(a)-3(c). As a result a mass gap is opened up in the electronic spectrum and the system is transformed from the 3D massless Weyl

semimetal to a quasi-2D massive Dirac metal. This is analyzed in Supplementary Materials (Part A). Such field induced Weyl points annihilation is a topological quantum phase transition and has never been reported experimentally before.

Now, we consider the orbital effect that couples to the motion in the  $a$ - $c$  plane when the system's Fermi energy approaches to zeroth Landau level. Due to the orbital effect, the energy of zeroth Landau level is shifted away from zero energy, as illustrated in Fig. 3(e). The detailed theoretical analysis of the orbital effect is shown in Supplementary Materials (Part A). This orbital splitting in 2D massive Dirac metal in the zero-mode LL is similar to the valley polarization of zeroth Landau level in transition metal dichalcogenides<sup>28-33</sup>, where the valleys shift in opposite directions under magnetic field due to the different chiralities. The observed nMR in Fig. 1(b) near 8 T, where system becomes a quasi-2D *massive* Dirac metal, is most probably triggered by this orbital effect while approaching the zeroth Landau level. Usually, semimetal has large MR due to particle-hole symmetry<sup>34</sup>. While due to the orbital effect, the zeroth LL shifts away from zero energy, correspondingly, the extra carriers will be introduced during this process and the particle-hole symmetry in the system is broken. Thus the MR would largely be suppressed, which will lead to an nMR. Also, the induced extra carriers during this process is demonstrated by Hall resistance in ZrTe<sub>5</sub> single crystal compound, as shown in Figure 4, where the Hall resistance shows an anomaly in nMR region, hinting extra carriers has been introduced by the orbital effect. As field increases, the nMR disappears near 14 T, followed by an upturn of the MR. This is due to the saturation of the orbital splitting, and the MR becomes positive

finally. As mentioned above, the band width for different samples of our bulk compounds ranges from 10 *meV* to 19 *meV*, correspondingly, the critical magnetic field needed for topological quantum phase transition ranges from 8 T to 18 T. This is also consistent with our observation, as shown in Supplementary materials (Supplementary Fig. 1), where nMR appears in different field region ranging from 8 T to 18 T for different single crystals. As the temperature increases, the peak position of MR moves to the high temperature region and disappears while T=80 K. This is because as T increases, the thermal fluctuation will smear out the orbital splitting gradually and correspondingly, a more intense magnetic field is needed to shift the zeroth LL.

Further evidence for the orbital splitting in high field region comes from the anisotropic magnetoresistance (AMR) in a rotating magnetic field, which provides a better insight on the anisotropy of the Fermi surface, as did in some other Dirac systems<sup>35-38</sup>. Figure 5 shows the AMR with B rotating *consecutively* in the *b-c* plane at an angle  $\varphi$  to *b*-axis. In layered material ZrTe<sub>5</sub>, the carrier in *a-c* plane has a maximal mobility and large MR, while in the other plane, the MR is much smaller than that in *a-c* plane<sup>39,40</sup>. Thus, as  $\varphi$  consecutively increases from 0° to 360°, the MR will change accordingly, and a 2-fold symmetry of AMR is formed in low field region (B<8 T).

While above 8 T, due to the orbital effect, the zeroth LL will shift away from zero energy consecutively as the increasing of the magnetic field. Correspondingly, the observed 2-fold symmetry exhibits a deformation and the peak position of the AMR

at  $\varphi = 0^\circ$  and  $180^\circ$  splits into two sub-peaks. With the further increase of the magnetic field, the split spacing, defined by the spacing of two sub-peaks, is enlarged, as shown in Fig. 5(a). This is because in the high field region, the Fermi surface on one hand becomes quasi-2D, on the other hand the orbital splitting will shift the zeroth LL away from zero energy, which will break the particle-hole symmetry and induce extra carriers and thus weaken the MR in this direction. When B is tilted away from *b*-axis to *c*-axis direction, the orbital splitting is largely decreased, considering that the orbital effect mainly happens for B along *b*-axis, and the MR will increase accordingly due to the sharp weakening of the orbital effect. As the tilted angle increasing to  $90^\circ$  (in-plane direction), the MR will decrease again due to the quasi-2D properties of the system in high field region where it has a small MR in in-plane direction. Thus the AMR, in comparison with low field region, exhibits a deformation in high field region. While B is up to 14 T, the orbital splitting is nearly saturated and the MR exhibits an upturn, correspondingly, the AMR near  $0^\circ$  and  $180^\circ$  shows a hump, as one can see in Fig. 5(a). As T increases, due to the thermal fluctuation, the orbital splitting is smeared out gradually and correspondingly, the deformation of the AMR is weakened, as we can see in Fig. 5(b)-5(e) for T= 10 K, 30 K, 50 K and 80 K respectively. While above 80 K, as shown in Fig. 5(f), the deformation of the AMR disappears even with B up to 16 T. Similar behavior can also be seen for magnetic field rotating in the *b*-*a* plane (Supplementary Fig. 2), where the AMR was obtained by rotating magnetic field in *b*-*a* plane under different temperatures. Similar to that with B rotating in *b*-*c* plane, the AMR exhibits a 2-fold symmetry in low field region,

while in high field region, the observed 2-fold symmetry of AMR exhibit a deformation, due to the orbital splitting.

In conclusion, we reported a field-induced topological phase transition from 3D Weyl semimetal to 2D massive Dirac metal in  $\text{ZrTe}_5$  when the Zeeman splitting exceeds the bandwidth along the layered direction (i.e., the  $b$ -axis). This is manifested by a sharp nMR and Hall anomaly above 8 T induced by the orbital effect. Further evidence is provided by the different AMR under various rotating magnetic fields. Our experiment reveals a magnetic field induced Weyl points annihilation, which can stimulate further research on field induced topological quantum phase transition in topological semimetal.

## Reference

1. Kim, H. J., Kim, K. S. *et al.* Dirac versus Weyl Fermions in topological insulators: Adler-Bell-Jackiw anomaly in transport phenomena. *Phys. Rev. Lett.* **111**, 246603 (2013).
2. Li, Q. *et al.* Chiral magnetic effect in  $\text{ZrTe}_5$ . *Nature Phys.* **12**, 550-554 (2016).
3. Huang, X. C. *et al.* Observation of the Chiral-Anomaly-Induced negative magnetoresistance in 3D Weyl semimetal TaAs. *Phys. Rev. X* **5**, 031023 (2015).
4. Li, H. *et al.* Negative magnetoresistance in Dirac semimetal  $\text{Cd}_3\text{As}_2$ . *Nature Commun.* **7**, 10301(2015).
5. Li, C. Z. *et al.* Giant negative magnetoresistance induced by the chiral anomaly in individual  $\text{Cd}_3\text{As}_2$  nanowires. *Nature Commun.* **6**, 10137 (2015).
6. Xiong, J. *et al.* Evidence for the chiral anomaly in the Dirac semimetal  $\text{Na}_3\text{Bi}$ . *Science* **350**, 413 (2015).
7. Zhang, C.-L. *et al.* Signatures of the Adler–Bell–Jackiw chiral anomaly in a Weyl

- Fermion semimetal. *Nature Commun.* **7**, 10735 (2016).
8. Yang, X. J. *et al.* Chiral anomaly induced negative magnetoresistance in topological Weyl semimetal NbAs. [arXiv:1506.03190](https://arxiv.org/abs/1506.03190).
  9. Arnold, F. *et al.* Negative magnetoresistance without well-defined chirality in the Weyl semimetal TaP. *Nature Commun.* **7**, 11615 (2016).
  10. Burkov, A. A., Balents, L. Weyl semimetal in a topological insulator multilayer. *Phys. Rev. Lett.* **107**, 127205 (2011).
  11. Burkov, A. A., Hook, M. D., Balents, L. Topological nodal semimetal. *Phys. Rev. B* **84**, 235126 (2011).
  12. Xu, G. *et al.* Chern semimetal and the quantized anomalous Hall effect in HgCr<sub>2</sub>Se<sub>4</sub>. *Phys. Rev. Lett.* **107**, 186806 (2011).
  13. Yang, K. Y. *et al.* Quantum Hall effects in a Weyl semimetal: Possible application in pyrochlore iridates. *Phys. Rev. B* **84**, 075129 (2011).
  14. Fang, C. *et al.* Multi-Weyl topological semimetals stabilized by point group symmetry. *Phys. Rev. Lett.* **108**, 266802 (2012).
  15. Young, S. M. *et al.* Dirac semimetal in three dimensions. *Phys. Rev. Lett.* **108**, 140405 (2012).
  16. Wang, Z. J. *et al.* Dirac semimetal and topological phase transitions in A<sub>3</sub>Bi (A = Na, K, Rb). *Phys. Rev. B* **85**, 195320 (2012).
  17. Wang, Z. J. *et al.*, Three-dimensional Dirac semimetal and quantum transport in Cd<sub>3</sub>As<sub>2</sub>. *Phys. Rev. B* **88**, 125427 (2013).
  18. Zyuzin, A. A. *et al.* Weyl semimetal with broken time reversal and inversion symmetries. *Phys. Rev. B* **85**, 165110 (2012).
  19. Chen, R. Y. *et al.*, Magnetoinfrared spectroscopy of Landau levels and Zeeman splitting of three-dimensional massless Dirac Fermions in ZrTe<sub>5</sub>. *Phys. Rev. Lett.* **115**, 176404 (2015).

20. Zheng, G. L. *et al.*, Transport evidence for the three-dimensional Dirac semimetal phase in ZrTe<sub>5</sub>. *Phys. Rev. B* **93**, 115414 (2016).
21. Wen, H. M., Dai, X., Fang, Z. Transition-Metal Pentatelluride ZrTe<sub>5</sub> and HfTe<sub>5</sub>: A paradigm for large-gap quantum spin Hall insulators. *Phys. Rev. X* **4**, 011002 (2014).
22. Chen, R. Y. *et al.* Optical spectroscopy study of the three-dimensional Dirac semimetal ZrTe<sub>5</sub>. *Phys. Rev. B* **92**, 075107 (2015).
23. Stillwell, E. P. *et al.* Effect of elastic tension on the electrical resistance of HfTe<sub>5</sub> and ZrTe<sub>5</sub>. *Phys. Rev. B* **39**, 1626 (1989).
24. Fang, F. F. *et al.* Effects of a tilted magnetic field on a two-dimensional electron gas. *Phys. Rev.* **174**, 823 (1968).
25. Linke, H. *et al.* Application of microwave detection of the Shubnikov-de Haas effect in two-dimensional systems. *J. Appl. Phys.* **73**, 7533 (1993).
26. Li, X. B. *et al.* Experimental observation of topological edge states at the surface step edge of the topological insulator ZrTe<sub>5</sub>. *Phys. Rev. Lett.* **116**, 176803 (2016).
27. Kamm, G. N. *et al.* Fermi surface, effective masses, and energy bands of HfTe<sub>5</sub> as derived from the Shubnikov-de Haas effect. *Phys. Rev. B* **35**, 1223 (1987).
28. Cai, T. Y. *et al.* Magnetic control of the valley degree of freedom of massive Dirac fermions with application to transition metal dichalcogenides. *Phys. Rev. B* **88**, 115140 (2013).
29. Srivastava, A. *et al.* Valley Zeeman effect in elementary optical excitations of monolayer WSe<sub>2</sub>. *Nature Phys.* **11**, 141-147 (2015).
30. Li, Y. L. *et al.* Valley splitting and polarization by the Zeeman effect in monolayer MoSe<sub>2</sub>. *Phys. Rev. Lett.* **113**, 266804 (2014).
31. Chu, R. L. *et al.* Valley-splitting and valley-dependent inter-Landau-level optical transitions in monolayer MoS<sub>2</sub> quantum Hall systems. *Phys. Rev. B* **90**, 045427 (2014).

32. MacNeill, D. *et al.* Breaking of valley degeneracy by magnetic field in monolayer MoSe<sub>2</sub>. *Phys. Rev. Lett.* **114**, 037401 (2015).
33. Aivazian, G. *et al.*, Magnetic control of valley pseudospin in monolayer WSe<sub>2</sub>. *Nature Phys.* **11**, 148-152 (2015).
34. Ali, M. N. *et al.* Large, non-saturating magnetoresistance in WTe<sub>2</sub>. *Nature* **514**, 205-208 (2014).
35. Zhu, Z. W. *et al.* Field-induced polarization of Dirac valleys in Bismuth. *Nature Phys.* **8**, 89 (2012).
36. Jo, Y. J. *et al.* Valley-polarized interlayer conduction of anisotropic Dirac Fermions in SrMnBi<sub>2</sub>. *Phys. Rev. Lett.* **113**, 156602 (2014).
37. Sulaev, A. *et al.* Electrically tunable in-plane anisotropic magnetoresistance in topological insulator BiSbTeSe<sub>2</sub> nanodevices. *Nano Lett.* **15**, 2061-2066 (2015).
38. Collaudin, A. *et al.* Angle dependence of the orbital magnetoresistance in Bismuth. *Phys. Rev. X* **5**, 021022 (2015).
39. Kamm, G. N. *et al.* Fermi surface, effective masses, and Dingle temperatures of ZrTe<sub>5</sub> as derived from the Shubnikov-de Haas effect. *Phys. Rev. B* **31**, 7617 (1985).
40. Tritt, T. M. *et al.* Large enhancement of the resistive anomaly in the pentatelluride materials HfTe<sub>5</sub> and ZrTe<sub>5</sub> with applied magnetic field. *Phys. Rev. B* **60**, 7816 (1999).

## Acknowledgments

This work was supported by the Natural Science Foundation of China (Grant No.11174294, 11574320, 11374302, 11204312, 11474289, U1432251 and U1332139), National Science Foundation of USA (Grant No.DMR-1442366 and DMR-1157490), and the CAS/SAFEA international partnership program for creative research teams of China.

## **Author contributions**

M. T., K. Y., W. N. and G. Z. conceived and designed the experiment. X. Z., J. Y., and H. D. fabricated the crystals; G. Z., X. Z., J. L, Y. H., H. Z and W. G performed the experiments under magnetic fields. The interpretation was developed by K.Y., G. Z., Y. Z., W. N., and M. T. The manuscript was prepared by G. Z., K. Y. and M. T., together with help of all other co-authors. All authors discussed the results and contributed to the manuscript.

## Figure Captions

### Figure 1 | Temperature dependent magnetoresistivity and the SdH oscillations in sample S1.

(a), the magnetoresistivity under different temperatures. A sharp drop of MR can be easily identified above 8 T at 2 K, and the peak position shifts to high field region as the increase of temperature. Inset is the schematic arrangement of the four-probe device, the current is injected along  $a$ -axis. (b), the SdH oscillation component as function of  $1/B$  at different temperatures. Both the  $n=2$  and  $n=1$  peaks exhibit the splitting. The observed LL splits are smeared out when the temperature is above 20 K.

### Figure 2|Angular dependent magnetoresistance (ADMR) in sample S1 at 2 K.

(a), the ADMR with  $B$  tilted in  $b$ - $a$  plane under different tilted angle  $\theta$ . (b), the angular dependence of the resistance oscillations versus  $1/B\cos(\theta)$ . (c) and (d) are respectively the ADMR and the resistance oscillations with  $B$  tilted in  $b$ - $c$  plane with an angle  $\varphi$  to  $b$ -axis.

### Figure 3|Zeeman splitting and Orbital effect.

(a)-(c), large Zeeman splitting will shift the Weyl points to Brillouin Zone boundary (upper figure), where the two Weyl points eventually meet and annihilate each other at the zone boundary (middle figure) and open a gap (lower figure). (d), a schematic illustration of the Landau levels of two Weyl nodes without the orbital effect. (e), a schematic illustration of the orbital splitting of the massive 2D Dirac metal for zeroth Landau level. Due to the orbital effect, the zeroth LL shifts, for example, downward (depending on the chirality of the Dirac point), and introduces extra carriers.

**Figure 4|Hall effect in sample S2.** In the nMR region, the Hall resistance exhibits an anomaly, reveals that extra carriers are induced due to the orbital effect.

**Figure 5|The AMR for S1 in  $b$ - $c$  plane by rotating magnetic field under different temperatures. (a)-(f) are respectively obtained at 2, 10, 30, 50, 80 and 180 K;**

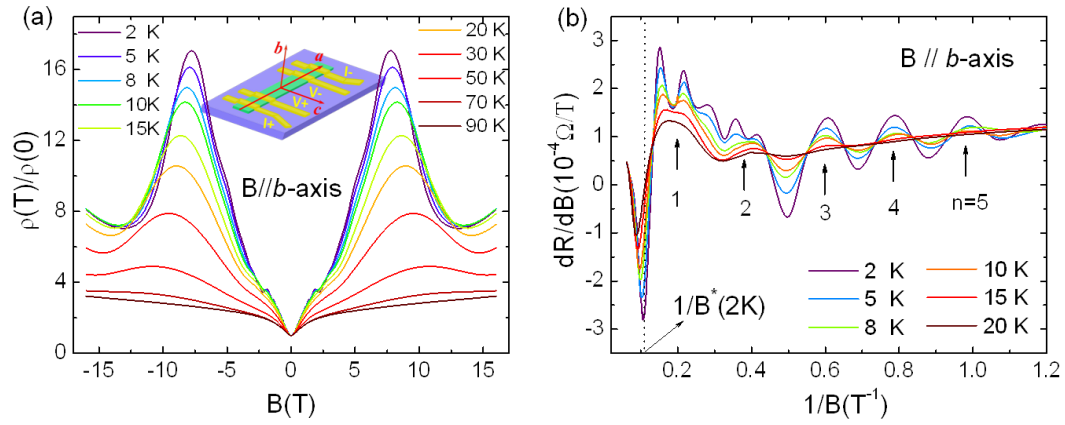


**Figure 1 | Temperature dependent magnetoresistivity and the SdH oscillations in sample S1.**

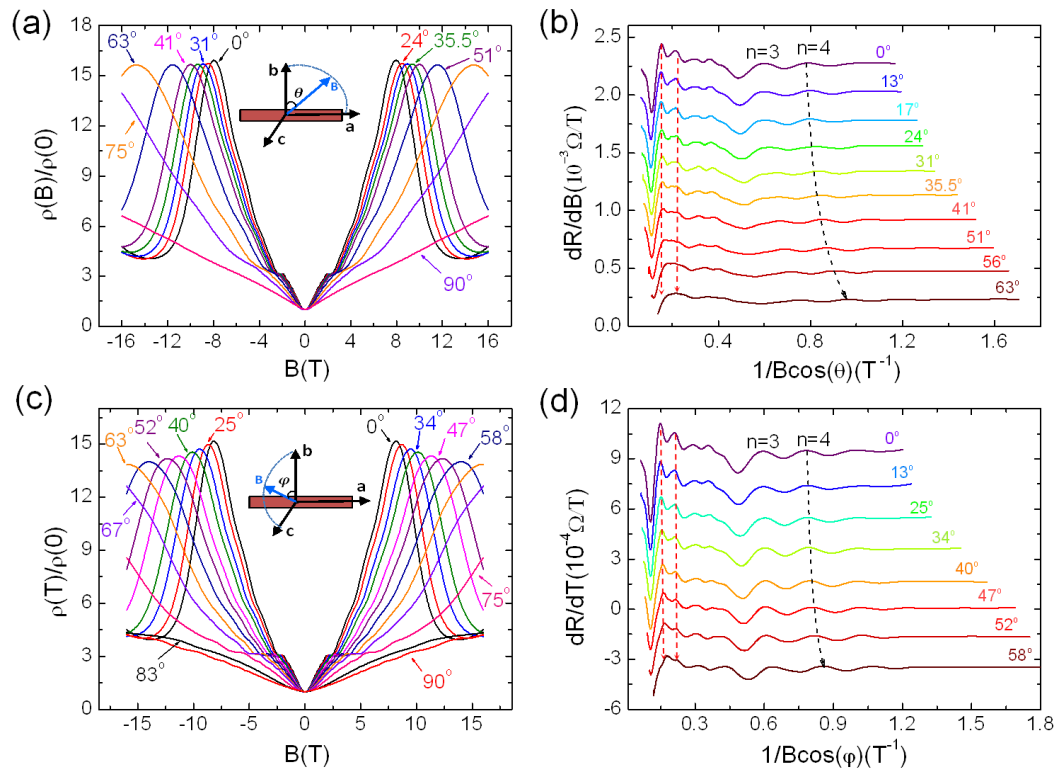


**Figure 2|Angular dependent magnetoresistance (ADMIR) in sample S1 at 2 K.**

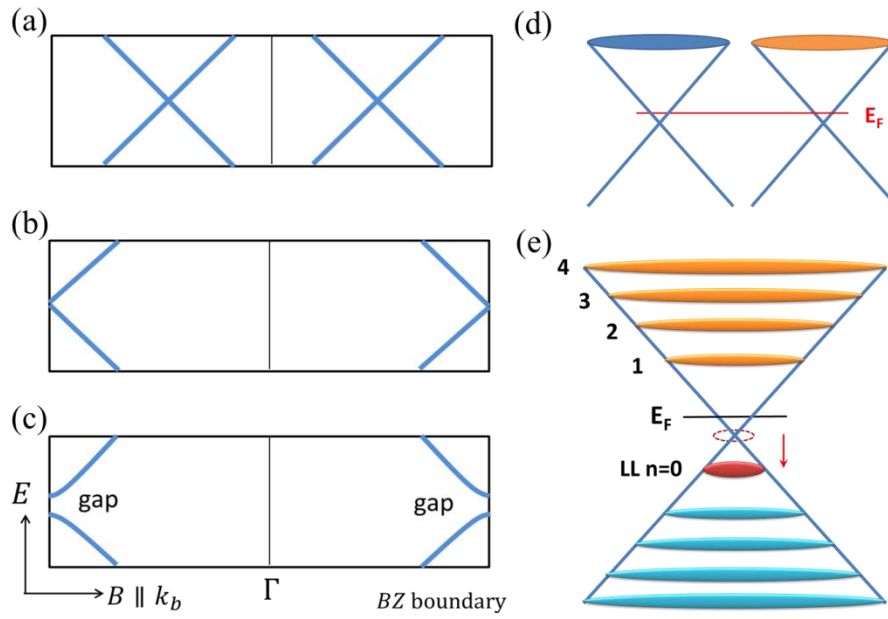


**Figure 3|Zeeman splitting and orbital effect.**

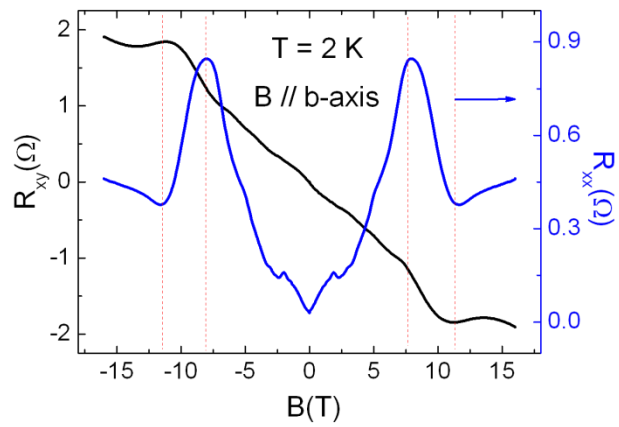


**Figure 4|Hall effect in sample S2.**

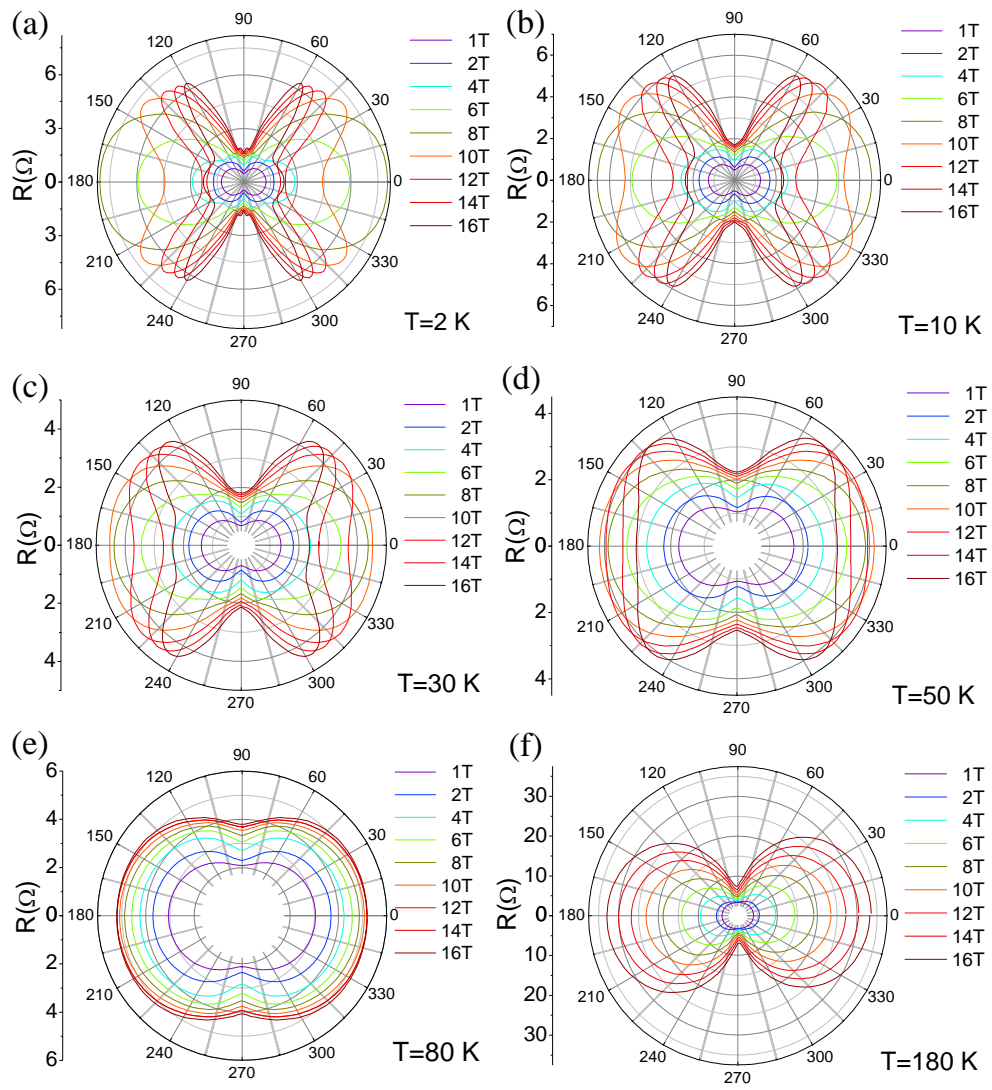


**Figure 5** The AMR for S1 in  $b$ - $c$  plane by rotating magnetic field under different temperatures. (a)-(f) are respectively obtained at 2, 10, 30, 50, 80 and 180 K;

# Supplementary Materials

## Part A. Orbital splitting of ZrTe<sub>5</sub> in quantum limit.

When the two Weyl points move toward each other and meet at the Brillouin zone boundary due to the large Zeeman splitting, the two Weyl points now need to be taken into account on equal footing. For simplicity we assume in the following that the velocity is isotropic and the annihilation of two Weyl points happens at  $\mathbf{k}=0$ , in which case the low-energy effective Hamiltonian near the annihilation transition is

$$H = v(\sigma_x p_x + \sigma_y p_y) - \sigma_z[\alpha k_z^2 + \beta(B - B^*)]. \quad (\text{A-1})$$

Here  $\alpha$  and  $\beta$  are constants assumed to be positive (the case when one or both of them are negative proceed in very similar manners).

For  $B < B^*$  there are two Weyl points at  $k_z = \pm\sqrt{\beta(B^* - B)}/\alpha$ , which merge at  $B = B^*$ . For  $B > B^*$  the coefficient of  $\sigma_z$  never vanishes and there is always a gap in the spectrum.

Now assuming the Zeeman splitting is large enough such that the dispersion along  $\hat{z}$  direction can be neglected so the system is effectively 2D-like, we have

$$H = v(\sigma_x p_x + \sigma_y p_y) - \Delta_z \sigma_z, \quad (\text{A-2})$$

which is the 2D massive Dirac Hamiltonian. In the presence of magnetic field we need to perform the standard minimum substitution of

$$\vec{p} \Rightarrow \vec{\Pi} = \vec{p} + e\vec{A}(\vec{r})/c, \quad (\text{A-3})$$

Where  $\vec{\Pi}$  is the mechanical momentum.

We have

$$H = \begin{pmatrix} -\Delta_Z & v(\Pi_x - i\Pi_y) \\ v(\Pi_x + i\Pi_y) & \Delta_Z \end{pmatrix} = \begin{pmatrix} -\Delta_Z & \epsilon_D a^+ \\ \epsilon_D a & \Delta_Z \end{pmatrix}, \quad (\text{A-4})$$

where

$$a = \frac{\ell}{\sqrt{2}\hbar}(\Pi_x + i\Pi_y), \quad a^+ = \frac{\ell}{\sqrt{2}\hbar}(\Pi_x - i\Pi_y), \quad (\text{A-5})$$

in which  $\ell = \sqrt{\hbar c/eB}$  is the magnetic length such that  $[a, a^+] = 1$ , and the parameter  $\epsilon_D = \sqrt{2}\hbar v/\ell$ .

The zeroth Landau level wave function of the Dirac point take the form of

$$\begin{pmatrix} |0\rangle \\ 0 \end{pmatrix}, \quad (\text{A-6})$$

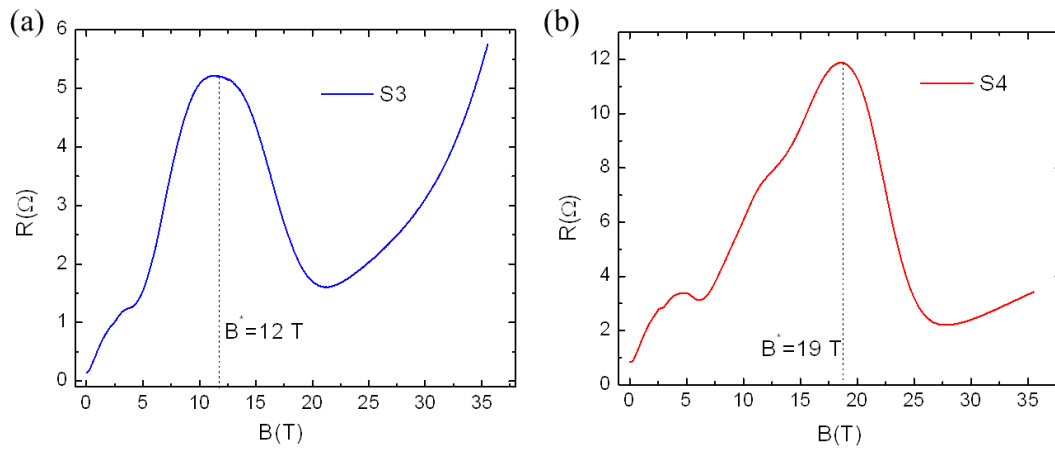
where  $|0\rangle$  is the usual harmonic oscillator ground state that is annihilated by  $a$ . The corresponding energy is  $-\Delta_Z$ . Thus the zeroth Landau level breaks the particle-hole symmetry in the energy spectrum. All the other Landau levels come in particle-hole symmetric pairs.

This is in sharp contrast to the case  $B < B^*$ , where in the Weyl semimetal phase the spectrum is strictly particle-hole symmetric, with or without the magnetic field. Thus the topological transition associated with the magnetic-field driven annihilation of the Weyl points reorganizes the electronic spectrum, induces additional carriers and leads to significant change in transport properties of the system including Hall effect.

## **Part B. The critical field for topological quantum phase transition in sample S3 and S4.**

We have measured different ZrTe<sub>5</sub> single crystal compound and find that, the nMR region happens at different field region. For the S1 and S2 discussed in main text, the critical field  $B^*$  is about 8 T, where the magnetoresistance (MR) exhibits a

peak. While for S3 and S4, as shown in Fig. A1, the critical field is about 12 T and 19 T respectively. We argue that this difference is due to the different crystal quality. As mentioned in main text, the calculated band width for different samples of our bulk compounds ranges from 10 meV to 19 meV, and correspondingly, the critical magnetic field needed for topological quantum phase transition might range from 8 T to 18 T, which is quantitatively constant with our observation.

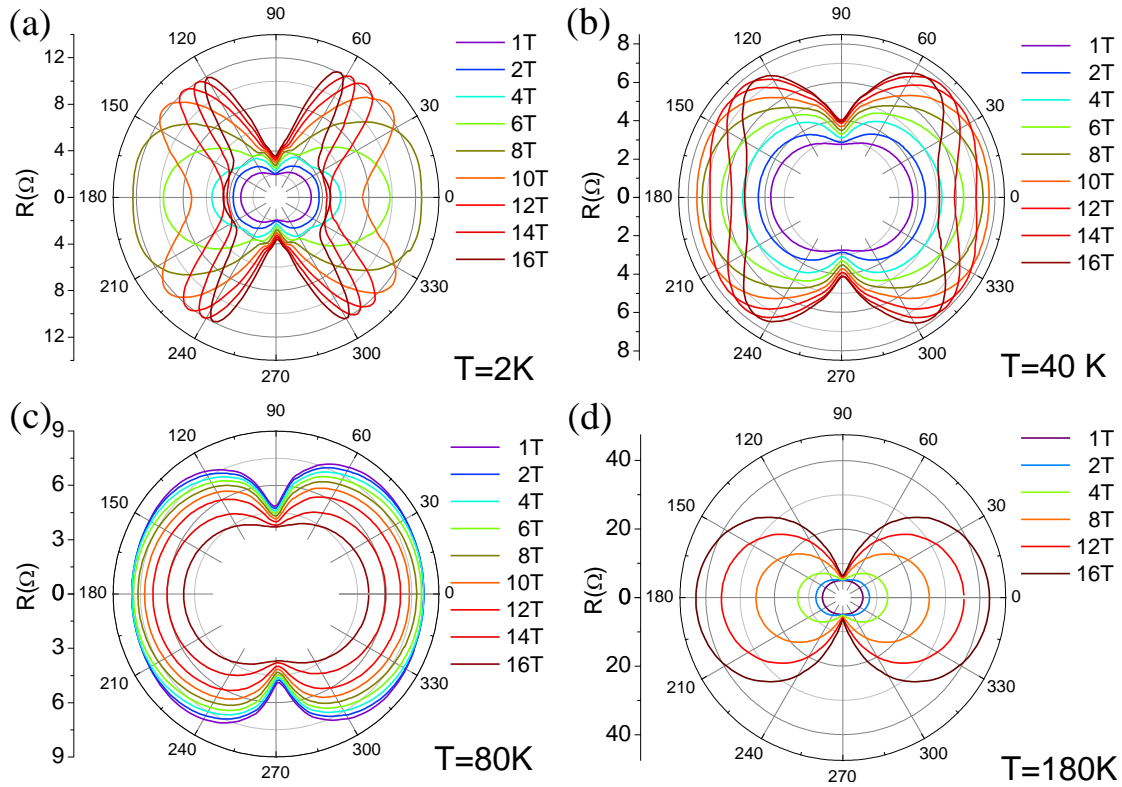


**Supplementary Figure 1 | The MR curves at 300 mK with  $B$  applied along  $b$ -axis for different samples.** (a) For S3, the MR exhibits a peak near 12 T, followed by a sharp drop of the MR. (b), for S4, the MR exhibits a peak near 19 T, followed by a sharp drop of the MR.

### Part C. The angular dependent Magnetoresistance (ADMR).

While rotating the magnetic field in the  $b$ - $a$  plane in S1, we find that, similar to that in  $b$ - $c$  plane, the ADMR in  $b$ - $a$  plane also exhibit a 2-fold symmetry in low field region. As  $B$  increased, the ADMR still keeps 2-fold symmetry till at 8 T, where a deformation of ADMR happens, as shown in Fig. A2. Similar to that in  $b$ - $c$  plane discussed in main text, the observed deformation of ADMR in high field region is caused by the orbital splitting, which induces extra carriers and leads to an nMR at high field region. As  $T$  increased, the deformation of ADMR is gradually suppressed

and disappeared while  $T > 80$  K, correspondingly, the ADMR exhibit a 2-fold symmetry even with B up to 16 T.



**Supplementary Figure 2 | The ADMR for S1 in  $b$ - $a$  plane in a rotating magnetic field under different temperatures. (a)-(d) are respectively obtained at 2, 40, 80 and 180 K.**